Braz J Phys (2011) 41:333–348
DOI 10.1007/s13538-011-0044-z

SBF SOCIEDADE BRASILEIRA DE FÍSICA

PARTICLES AND FIELDS

A Modified Generalized Chaplygin Gas as the Unified Dark Matter–Dark Energy Revisited

Xue-Mei Deng

Received: 9 August 2011 / Published online: 21 September 2011

Abstract A modified generalized Chaplygin gas (MGCG) is considered as the unified dark matter–dark energy revisited. The character of MGCG is endued with the dual role, which behaves as matter at early times and as a quiessence dark energy at late times. The equation of state for MGCG is $p = -\alpha\rho/(1+\alpha) - \vartheta(z)\rho^{-\alpha}/(1+\alpha)$, where $\vartheta(z) = -[\rho_{0c}(1+z)^3]^{(1+\alpha)}(1-\Omega_{0B})^{\alpha}\{\alpha\Omega_{0DM} + \Omega_{0DE}[\omega_{DE} + \alpha(1+\omega_{DE})](1+z)^{3\omega_{DE}(1+\alpha)}\}$. Some cosmological quantities, such as the densities of different components of the universe Ω_i (i, respectively, denotes baryons, dark matter, and dark energy) and the deceleration parameter q, are obtained. The present deceleration parameter q_0, the transition redshift z_T, and the redshift z_{eq}, which describes the epoch when the densities in dark matter and dark energy are equal, are also calculated. To distinguish MGCG from others, we then apply the Statefinder diagnostic. Later on, the parameters (α and ω_{DE}) of MGCG are constrained by combination of the sound speed c_s^2, the age of the universe t_0, the growth factor m, and the bias parameter b. It yields $\alpha = -3.07^{+5.66}_{-4.98} \times 10^{-2}$ and $\omega_{DE} = -1.05^{+0.06}_{-0.11}$. Through the analysis of the growth of density perturbations for MGCG, it is found that the energy will transfer from dark matter to dark energy which reach equal at $z_{eq} \sim 0.48$ and the density fluctuations start deviating from the linear behavior at $z \sim 0.25$ caused by the dominance of dark energy.

Keywords Dark energy · Dark matter

X.-M. Deng (✉)
Purple Mountain Observatory,
Chinese Academy of Sciences, Nanjing 210008, China
e-mail: xmd@pmo.ac.cn

1 Introduction

As standardized candles, type Ia supernovae suggest that the universe is undergoing accelerating expansion [1–3]. The same evidence has been shown by cosmic microwave background (CMB) [4, 5] and large-scale structure (LSS) [6] observations. All these data indicate that the dominant component of the universe is relatively smooth and has a large negative pressure. All kinds of alternative models stand up for explaining this exotic phenomena within relativistic theory of gravity, which include the energy of the quantum vacuum (such as cosmological constant Λ [7, 8]), the existence of another new scalar field (quintessence [9–11] which is possibly related to the inflaton, k-essence [12–14], tachyon [15–17], phantom [18–20], and quintom [21, 22]), and the influence of unseen additional spatial dimensions predicted by string theory [23–25]. Instead of the presence of dark energy, the most interesting idea for solving this dark riddle depend on a new aspect of gravity which is not accounted for general relativity [26, 27]. Unfortunately, the current astronomical observations data still cannot determine completely the nature of dark energy or decide its existence since this problem has puzzled us for a long time.

As one of plausible dynamical models for dark energy, Chaplygin gas (CG) and the generalized Chaplygin gas (GCG) [28–33] have created a lot of interest in recent times [34–37]. CG or GCG behaves like pressureless dust at early times and like a cosmological constant during very late times. The fact that the properties of CG and GCG interpolate between those of cold dark matter (CDM) and a Λ-term makes the models to provide a conceptual framework for a unified model of dark matter and dark energy. Besides, it is

more instructive to note that the GCG model has been successfully confronted with various phenomenological tests such as high precision CMB data, supernovae data, and gravitational lensing [38, 39]. On the other hand, since observations such as SNe Ia [1–3] are still not sufficient to establish evidence of a dynamical equation of state for dark energy, we can naturally consider a fluid consisted of dark matter and quiessence dark energy with constant $\omega_{\rm DE}$ which fill the whole universe. Thus, we propose a modified generalized Chaplygin gas (MGCG) as the unified dark matter and dark energy revisited on some previous works [40–42].

With future deeper and more intensive surveys of SNe Ia, such as supernovae acceleration probe (SNAP) [43], there will be a chance to distinguish different models of dark energy so that we will consider the so-called geometrical or Statefinder diagnostic since it can probe the expansion dynamics of the universe through higher derivatives of the scale factor. So, we must constrain the parameters (α and $\omega_{\rm DE}$) of the MGCG at first. The plan of this paper is as follows: In Section 2, we give corresponding fundamental cosmology equations about MGCG. Subsequently, in Section 3, we consider Statefinder diagnostic of the MGCG. We then constrain the parameters of the MGCG by means of the sound speed c_s^2, the age of the universe t_0, the growth factor m, and the bias parameter b in Section 4. Finally, conclusion and our results are outlined in Section 5.

2 Fundamental Cosmology Equations About MGCG

2.1 Motivation

An interesting unified model for two dark sectors is the CG model [44] introduced with $p=-A/\rho$. Although this model has been very successful in explaining the SNe Ia data, it shows that CG model does not pass the tests connected with structure formation and observed strong oscillations of the matter power spectrum [45, 46]. This situation can be alleviated in the GCG proposed with $p=-A/\rho^{\alpha}$. And the parameter α is rather severely constrained, i.e., $0\leq\alpha<0.2$ at the 95% confidence level [28–33]. Since the difference between ΛCDM and GCG models is so tiny and the equation of state of dark energy still cannot be determined exactly, a new generalized Chaplygin gas (NGCG) [42] was proposed by considering that A in GCG is a function of redshift z. Following this idea, we develop GCG-like models from another view. As a purely kinetic k-essence model with a constant potential, the tachyon fields can be considered as CG model [40]. Meanwhile, the tachyon field can also act as a source of dark energy depending upon the form of the tachyon potential. Thus, the authors in [41, 47] introduced an extended tachyon field (ETF) and then provided a modified Chaplygin gas (MCG) [41, 47], in which the equation of state (EOS) has a more generalized form

$$p=-\frac{\alpha}{1+\alpha}\rho-\frac{1}{1+\alpha}\frac{A}{\rho^{\alpha}}, \tag{1}$$

where A and α are constants. As a kind of new attempt just like the extension from GCG to NGCG, we present a MGCG through replacing A in (1) with a function $\vartheta(z)$ of redshift z. The analysis and discussion of the matter power spectrum for MGCG will be investigated in our future work by comparing the model with observations.

2.2 Deduction of Some Cosmological Quantities and Discussion

Within the framework of Friedmann–Robertson–Walker (FRW) cosmology, we consider an exotic background fluid called MGCG whose equation of state is as follows based on: [41, 47]

$$p=-\frac{\alpha}{1+\alpha}\rho-\frac{1}{1+\alpha}\frac{\vartheta(z)}{\rho^{\alpha}}, \tag{2}$$

where α is a constant and $\vartheta(z)$ is a function of redshift z. Since the MGCG is another new unified model with two dark sectors (namely, at early times the energy density behaves as dark matter: $\rho\propto(1+z)^3$, while at late times it behaves like a quiessence dark energy: $\rho\propto(1+z)^{3(1+\omega_{\rm DE})}$), it could be supposed the energy density of the MGCG as follows:

$$\rho=[\kappa(1+z)^{3(1+\alpha)}+\lambda(1+z)^{3(1+\omega_{\rm DE})(1+\alpha)}]^{\frac{1}{1+\alpha}}, \tag{3}$$

where the parameter of state for dark energy $\omega_{\rm DE}$ is a constant and should be taken as any value in the range $(-1.46,-0.78)$ [48, 49]. In Section 4, we will further constrain the $\omega_{\rm DE}$ in our model. Then the pressure of MGCG yields

$$p=-\frac{\alpha\left[\kappa\,(1+z)^{3(1+\alpha)}+\lambda\,(1+z)^{3(1+\omega_{\rm DE})(1+\alpha)}\right]+\vartheta(z)}{(1+\alpha)\left[\kappa\,(1+z)^{3(1+\alpha)}+\lambda\,(1+z)^{3(1+\omega_{\rm DE})(1+\alpha)}\right]^{\alpha/(1+\alpha)}}. \tag{4}$$

On the other hand, the whole pressure $p_{\rm total}$ and energy density $\rho_{\rm total}$ satisfy the conservation equation

$$\dot{\rho}_{\rm total}+3H\left(\rho_{\rm total}+p_{\rm total}\right)=0. \tag{5}$$

According to conservation of baryons, the continuity equation is separated into two parts:

$$\dot{\rho}_{\rm B}+3H\left(\rho_{\rm B}+p_{\rm B}\right)=0, \tag{6}$$

$$\dot{\rho} + 3H(\rho + p) = 0, \tag{7}$$

where subscript "B" denotes baryons. Using the (3), (4), and (7), we obtain

$$\vartheta(z) = -\Big\{[\omega_{\rm DE} + \alpha(1+\omega_{\rm DE})]\lambda(1+z)^{3(1+\omega_{\rm DE})(1+\alpha)} + \alpha\kappa(1+z)^{3(1+\alpha)}\Big\}. \tag{8}$$

Furthermore, the pressure of dark energy $p_{\rm DE}$, the energy density of dark energy $\rho_{\rm DE}$, and the one of dark matter $\rho_{\rm DM}$ can be, respectively, written as

$$p_{\rm DE} = p = \frac{\omega_{\rm DE}\lambda(1+z)^{3(1+\omega_{\rm DE})(1+\alpha)}}{\left[\kappa(1+z)^{3(1+\alpha)} + \lambda(1+z)^{3(1+\omega_{\rm DE})(1+\alpha)}\right]^{\alpha/(1+\alpha)}}, \tag{9}$$

$$\rho_{\rm DE} = \frac{p_{\rm DE}}{\omega_{\rm DE}} = \frac{\lambda(1+z)^{3(1+\omega_{\rm DE})(1+\alpha)}}{\left[\kappa(1+z)^{3(1+\alpha)} + \lambda(1+z)^{3(1+\omega_{\rm DE})(1+\alpha)}\right]^{\alpha/(1+\alpha)}}, \tag{10}$$

$$\rho_{\rm DM} = \rho - \rho_{\rm DE} = \frac{\kappa(1+z)^{3(1+\alpha)}}{\left[\kappa(1+z)^{3(1+\alpha)} + \lambda(1+z)^{3(1+\omega_{\rm DE})(1+\alpha)}\right]^{\alpha/(1+\alpha)}}. \tag{11}$$

From (3), (10), and (11), it gives that

$$\kappa + \lambda = \rho_0^{1+\alpha} = (\rho_{0\rm DM} + \rho_{0\rm DE})^{1+\alpha} = \rho_{0\rm C}^{1+\alpha}\left[1 - \Omega_{0\rm B}\right]^{1+\alpha}, \tag{12}$$

$$\rho_{0\rm DM} = \frac{\kappa}{[\kappa+\lambda]^{\alpha/(1+\alpha)}}, \tag{13}$$

$$\rho_{0\rm DE} = \frac{\lambda}{[\kappa+\lambda]^{\alpha/(1+\alpha)}}, \tag{14}$$

where $\rho_{0\rm C}$, ρ_0, $\rho_{0\rm DM}$, and $\rho_{0\rm DE}$ are the present values of $\rho_{\rm total}$, ρ, $\rho_{\rm DM}$, and $\rho_{\rm DE}$, respectively, and the label "0" denotes today's evaluated quantities. Parameters κ and λ can then be written as

$$\kappa = \Omega_{0\rm DM}\rho_{0\rm C}^{1+\alpha}\left[1-\Omega_{0\rm B}\right]^{\alpha}, \quad \lambda = \Omega_{0\rm DE}\rho_{0\rm C}^{1+\alpha}\left[1-\Omega_{0\rm B}\right]^{\alpha}. \tag{15}$$

Substituting (15) to (8), we have

$$\vartheta(z) = -\rho_{0\rm C}^{1+\alpha}\left[1-\Omega_{0\rm B}\right]^{\alpha}(1+z)^{3(1+\alpha)} \times \{\alpha\Omega_{0\rm DM} + \Omega_{0\rm DE}\left[\omega_{\rm DE} + \alpha\left(1+\omega_{\rm DE}\right)\right] \times (1+z)^{3\omega_{\rm DE}(1+\alpha)}\}. \tag{16}$$

Then, the equation of state for the MGCG model reads as

$$\chi(z) \equiv \frac{p}{\rho} = \frac{\omega_{\rm DE}\Omega_{0\rm DE}(1+z)^{3(1+\omega_{\rm DE})(1+\alpha)}}{\Omega_{0\rm DM}(1+z)^{3(1+\alpha)} + \Omega_{0\rm DE}(1+z)^{3(1+\omega_{\rm DE})(1+\alpha)}}. \tag{17}$$

The values of $\Omega_{0\rm DM}$ and $\Omega_{0\rm DE}$ depend on the model used in the data precessing. For example, both the Wilkinson Microwave Anisotropy Probe (WMAP) [50] and two-degree field Galaxy Redshift Survey (2dFGRS) [51] used ΛCDM model of the universe. Besides, cosmological parameters are also constrained with other models. In this paper, the current density parameters used in the plots are $\Omega_{0\rm B} = 0.0449 \pm 0.0028$, $\Omega_{0\rm DM} = 0.222 \pm 0.026$, and $\Omega_{0\rm DE} = 0.734 \pm 0.029$ based on WMAP7 data [50]. Later, we will give the constraints of α and $\omega_{\rm DE}$ in Section 4. From (17), we can plot the function $\chi(z)$ as the function of redshift z (see Fig. 1). $\chi(z)$ is always negative from past to future. And we can see the effect of the parameter α and $\omega_{\rm DE}$ on the $\chi(z)$. The evolution of $\chi(z)$ is mostly flat in the high redshift $z > 1$ and is very steep as redshift z becomes low.

When we consider a spatially flat FRW universe with the exotic background MGCG fluid and the baryon component, the Friedmann equation can be written as:

$$H^2 = \frac{8\pi G}{3}\rho_{\rm total}. \tag{18}$$

Then, we obtain

$$E^2(z) \equiv \frac{H^2}{H_0^2} = (1-\Omega_{0\rm B})^{\frac{\alpha}{1+\alpha}} \times\left[\Omega_{0\rm DM}(1+z)^{3(1+\alpha)} + \Omega_{0\rm DE}(1+z)^{3(1+\omega_{\rm DE})(1+\alpha)}\right]^{\frac{1}{1+\alpha}} + \Omega_{0\rm B}(1+z)^3. \tag{19}$$

The evolution of the Hubble parameter in units of $H_{\Lambda\rm CDM}$ is plotted in Fig. 2. During the cosmological evolution, the behavior of H is similar to $H_{\Lambda\rm CDM}$ at very early time, and when $z \to 0$, H is approaching ΛCDM.

By using the above equations, the densities of different components of the universe $\Omega_{\rm DM}$, $\Omega_{\rm DE}$, and $\Omega_{\rm B}$ can be, respectively, derived as

$$\Omega_{\rm DM} = \frac{(1-\Omega_{0\rm B})^{\frac{\alpha}{1+\alpha}}\,\Omega_{0\rm DM}(1+z)^3}{E^2(z)\left[\Omega_{0\rm DM} + \Omega_{0\rm DE}(1+z)^{3\omega_{\rm DE}(1+\alpha)}\right]^{\alpha/(1+\alpha)}}, \tag{20}$$

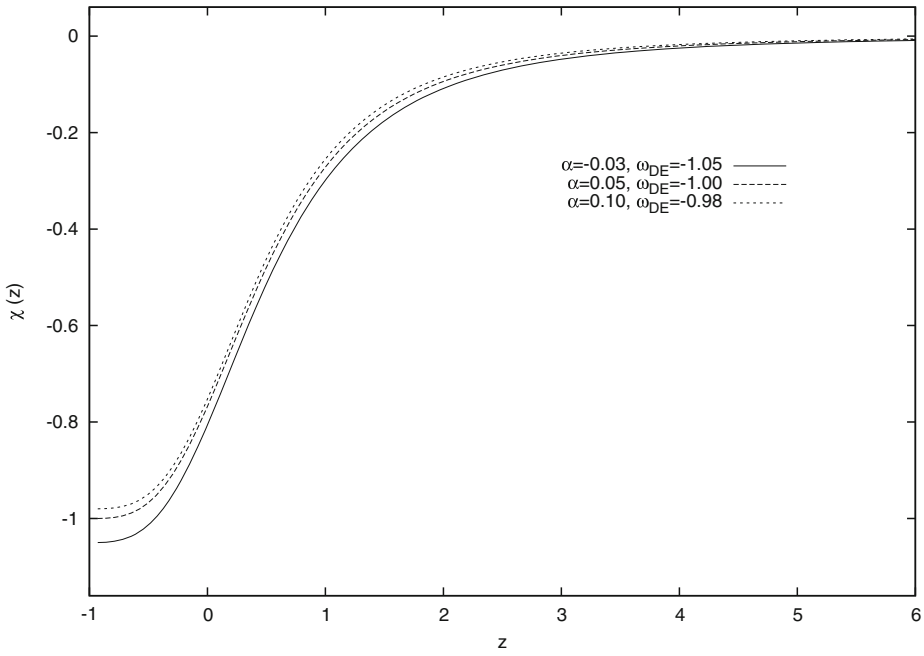

Fig. 1 The equation of state for the MGCG $\chi(z)$ as the function of redshift. Where $\Omega_{0\mathrm{B}} = 0.0449$, $\Omega_{0\mathrm{DM}} = 0.222$, and $\Omega_{0\mathrm{DE}} = 0.734$

$$\Omega_{\mathrm{DE}} = \frac{(1-\Omega_{0\mathrm{B}})^{\frac{\alpha}{1+\alpha}}\,\Omega_{0\mathrm{DE}}(1+z)^{3(1+\omega_{\mathrm{DE}})}}{E^2(z)\left[\Omega_{0\mathrm{DM}}(1+z)^{-3\omega_{\mathrm{DE}}(1+\alpha)}+\Omega_{0\mathrm{DE}}\right]^{\alpha/(1+\alpha)}}, \tag{21}$$

$$\Omega_{\mathrm{B}} = \frac{\Omega_{0\mathrm{B}}(1+z)^3}{E^2(z)}. \tag{22}$$

The relationships between Ω_i (i, respectively, denotes baryons, dark matter, and dark energy) and redshift z are shown in Fig. 3 with the prior of $\Omega_{0\mathrm{DM}} = 0.222$, $\Omega_{0\mathrm{DE}} = 0.734$, and $\Omega_{0\mathrm{B}} = 0.0449$. Based on Fig. 3, the evolutions of baryons, dark matter, and dark energy under MGCG model are consistent with what are

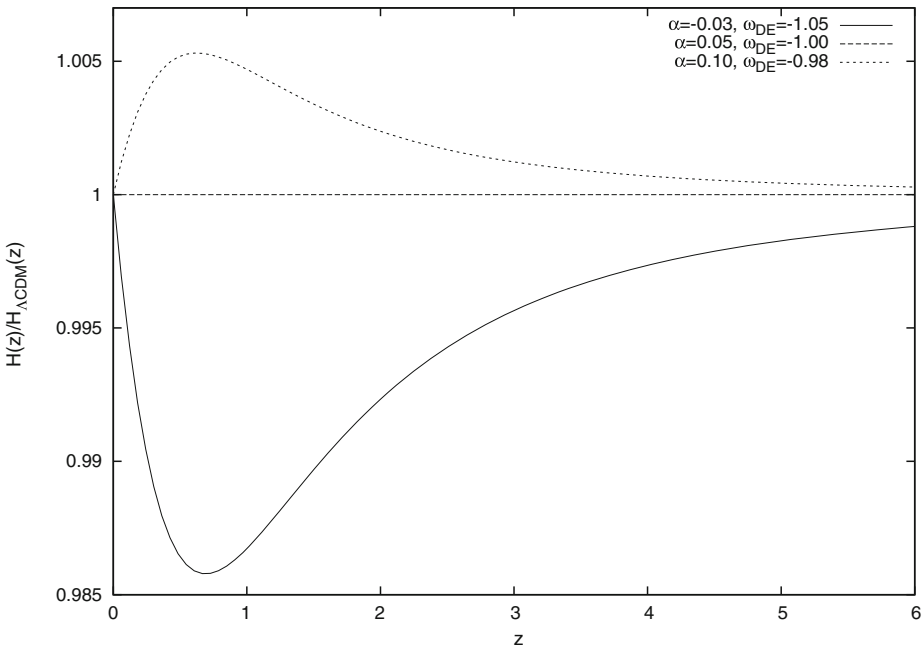

Fig. 2 The Hubble parameter in units of $H_{\Lambda\mathrm{CDM}}$ for the MGCG as the function of redshift. The priors $\Omega_{0\mathrm{DM}} = 0.222$, $\Omega_{0\mathrm{DE}} = 0.734$, and $\Omega_{0\mathrm{B}} = 0.0449$ have been used

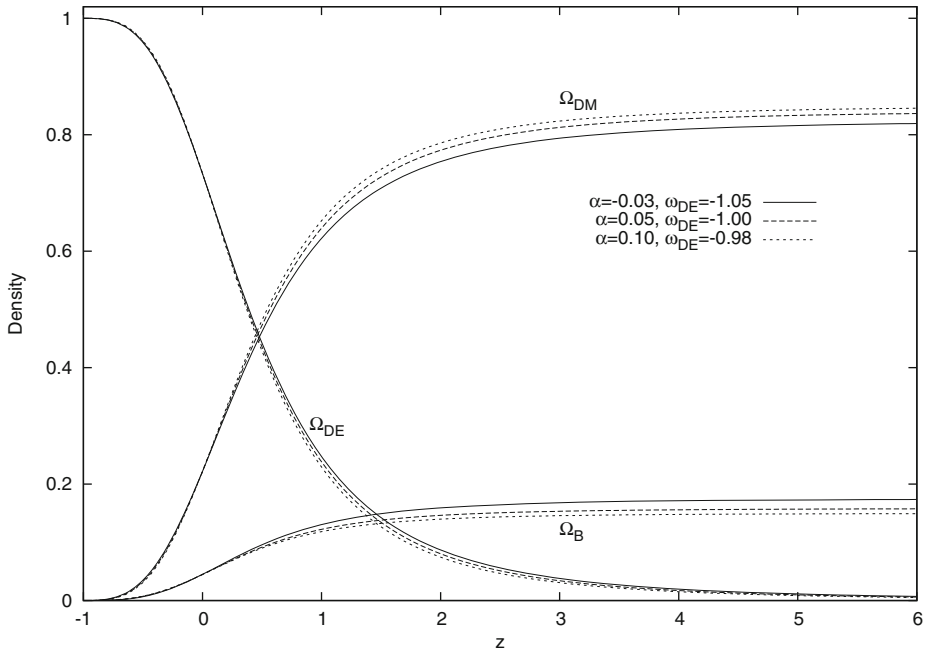

Fig. 3 The densities of Ω_{DE}, Ω_{DM}, and Ω_B as the functions of redshift

recognized [48, 49, 52, 53]. A very important redshift described the epoch when the densities in dark matter and dark energy are equal is $(1+z_{eq})^{-3\omega_{DE}(1+\alpha)} = \Omega_{0DE}/\Omega_{0DM}$. And $z_{eq} \simeq 0.48$ for $\alpha = -0.03, \omega_{DE} = -1.05$, $z_{eq} \simeq 0.46$ for $\alpha = 0.05, \omega_{DE} = -1.00$, and $z_{eq} \simeq 0.45$ for $\alpha = 0.10, \omega_{DE} = -0.98$, respectively. From Fig. 3, we also know that the dominance of the dark energy leads to the acceleration expansion of our universe. The increasing density of dark energy is the reason why expansion of our universe transited from

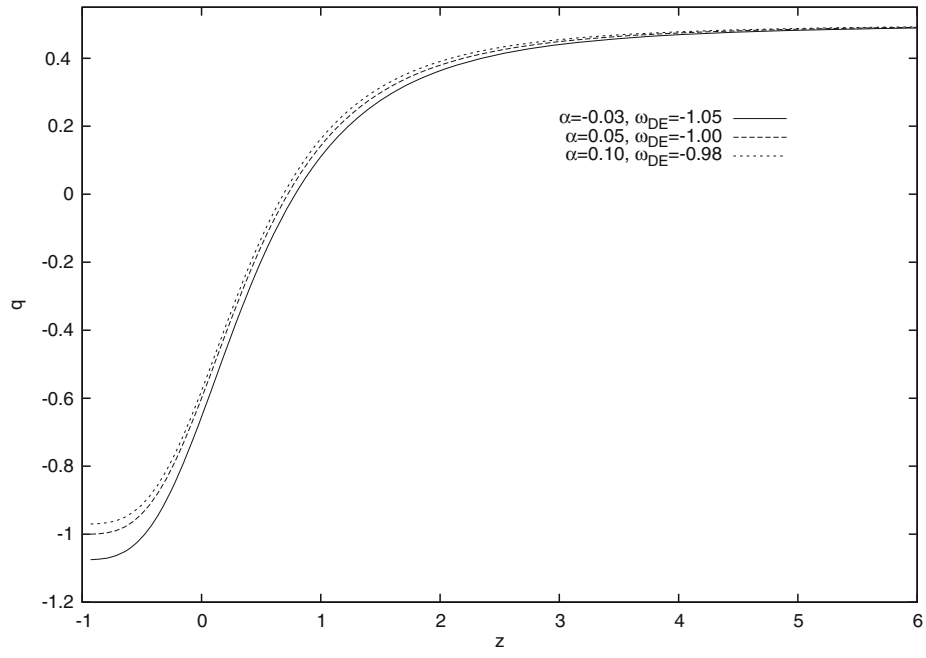

Fig. 4 The deceleration parameter q as the function of redshift. The priors $\Omega_{0DM} = 0.222$, $\Omega_{0DE} = 0.734$, and $\Omega_{0B} = 0.0449$ have been used

Table 1 Compare CG, GCG, NGCG, MCG, and MGCG

Models	EOS	A	Parameter(s)	$\rho_{\rm DM}/\rho_{\rm DE}$
CG	$p=-\frac{A}{\rho}$	Const.	A	$\sim(1+z)^3$
GCG	$p=-\frac{A}{\rho^\alpha}$	Const.	A and α	$\sim(1+z)^{3(1+\alpha)}$
NGCG	$p=-\frac{\tilde{A}(z)}{\rho^\alpha}$	Function of z	$\omega_{\rm DE}$ and α	$\sim(1+z)^{-3\omega_{\rm DE}(1+\alpha)}$
MCG	$p=-\frac{\alpha}{1+\alpha}\rho-\frac{1}{1+\alpha}\frac{A}{\rho^\alpha}$	Const.	A and α	$\sim(1+z)^{3(1+\alpha)}$
MGCG	$p=-\frac{\alpha}{1+\alpha}\rho-\frac{1}{1+\alpha}\frac{\vartheta(z)}{\rho^\alpha}$	Function of z	$\omega_{\rm DE}$ and α	$\sim(1+z)^{-3\omega_{\rm DE}(1+\alpha)}$

deceleration to acceleration. This transition will be described by our model in more detail with the deceleration parameter q.

The deceleration parameter is

$$\begin{aligned} q &\equiv -\frac{\ddot{a}}{aH^2} \\ &= -1-\frac{\dot{H}}{H^2} \\ &= -1+\frac{3(1+z)^3}{2E^2(z)}\left(1-\Omega_{0\rm B}\right)^{\alpha/(1+\alpha)} \\ &\quad\times\left\{\left[\Omega_{0\rm DM}+\Omega_{0\rm DE}(1+z)^{3\omega_{\rm DE}(1+\alpha)}\right]^{-\frac{\alpha}{1+\alpha}}\right. \\ &\quad\times\left[\Omega_{0\rm DM}+(1+\omega_{\rm DE})\,\Omega_{0\rm DE}(1+z)^{3\omega_{\rm DE}(1+\alpha)}\right] \\ &\quad\left.+\Omega_{0\rm B}\right\}. \end{aligned} \tag{23}$$

Thus, we can give the following results: The present deceleration parameter $q_0\approx-0.65$ according to $z=0$ and the transition redshift $z_{\rm T}\approx0.70$ according to $q=0$ when taking $\alpha=-0.03$, $\omega_{\rm DE}=-1.05$, $q_0\approx-0.60$, and $z_{\rm T}\approx0.65$ for $\alpha=0.05$, $\omega_{\rm DE}=-1.00$ and $q_0\approx-0.58$ and $z_{\rm T}\approx0.60$ for $\alpha=0.10$, $\omega_{\rm DE}=-0.98$, which are consistent with observations. The deceleration parameter as the function of redshift is shown in Fig. 4. According to Fig. 4, the expansion of the universe is from slowing down ($q>0$) in the past to speeding up ($q<0$) at present time and in the future. And when $q>0$ is at the high redshift, q changes very slow with redshift z; when $q<0$ is at the recent time, q changes faster and faster with redshift z.

Now, we compare some cosmological characters between CG, GCG, NGCG, MCG, and MGCG (see Table 1). In order to distinguish these model, we use the same symbols as above. From Table 1, we can see the EOSs of these models so that they have some different characters. First of all, CG and GCG can be treated as a unified fluid that behaves like pressureless dust at early times and like a cosmological constant during very late times. For NGCG, it is considered as X-CDM, where X means quiessence, since the authors in [42] extended A of GCG model. And MCG is the mixture of a barotropic perfect fluid and a generalized Chaplygin gas. At the same time, considering A of (1) changed with redshift z, we proposed MGCG.

Among them, GCG is an extended model of CG. When $\alpha=1$, GCG model becomes CG. And NGCG is an extended model of GCG. When $\tilde{A}(z)=$ const., NGCG reduces to GCG. MGCG is an extended version of MCG. When $\vartheta(z)=$ const., MGCG yields MCG. Meanwhile, both GCG and MCG can be conceived as ETF, in which GCG corresponds to the simplest model driven by a constant potential [41, 47]. It is worth to note that CG, GCG, NGCG, MCG, and MGCG are all interactive models. Namely, there are energy exchange between dark matter and dark energy. Basically, the behavior of the energy exchange can be presented as $\rho_{\rm DM}/\rho_{\rm DE}$. We can see that the transfer direction of the energy flow for CG is from dark matter to dark energy. However, the transfer direction of the energy flow for the others only depend on the parameter α if $\alpha\neq0$. When $\alpha>0$, the transfer direction of the energy flow is from dark matter to dark energy. When $\alpha<0$, the direction of transfer is inverse. Thus, constraints of parameters such as α and $\omega_{\rm DE}$ from observational data and theoretical analysis will play an important role in understanding the physical nature of these models. For GCG, authors in [55] obtain $\alpha<10^{-5}$ or $\alpha\geq3$ (the sound speed is larger than the speed of light) by using gauge-invariant analysis of perturbation. For NGCG, constraints of parameters are $1+\alpha=1.06^{+0.20}_{-0.16}$ and $\omega_{\rm DE}=-0.98^{+0.15}_{-0.20}$ by observational constraints from SNe Ia, CMB, and LSS data [42]. In Section 4, we will constrain α and $\omega_{\rm DE}$ in our model by the maximum likelihood estimation.

3 Statefinder Diagnostic

Dark energy models such as the cosmological constant [7, 8], quintessence [9–11], k-essence [12–14], Chaplygin gas [28–33], quintom [21, 22], etc. have properties which can be model dependent. In order to distinguish

the very distinct and competing cosmological scenarios involving dark energy, a sensitive and robust diagnostic of dark energy is needed. So a new diagnostic of dark energy called "Statefinder" diagnostic has been constructed by Sahni et al. [56] and Alam et al. [57] who were using both the second and the third derivatives of the scale factor a.

The statefinder pair $\{r, s\}$, in addition to the oldest and most well-known geometric variables H and q, defines two new cosmological parameters

$$r \equiv \frac{\dddot{a}}{aH^3}, \tag{24}$$

$$s \equiv \frac{r-1}{3(q-1/2)}. \tag{25}$$

An important property of the Statefinder is that spatially flat ΛCDM corresponds to the fixed point

$$\{r, s\}|_{\Lambda\mathrm{CDM}} = \{1, 0\}. \tag{26}$$

Clearly an important requirement of any diagnostic is that it permits us to tell the difference between a given dark energy model and the simplest of all models—the cosmological constant just as demonstrated in [50, 51, 54–59]. By using the $r(s)$ evolution diagram, the discrimination between a given dark energy model and the ΛCDM scenario can be clearly identified. And it is more worth to note that the Statefinder diagnostic combined with future SNAP [43] observations may possibly be used to distinguish between different dark energy models.

Based on the (24) and (25), we obtain the Statefinder parameters for the MGCG as follows:

$$r = 1 + 3\frac{\dot{H}}{H^2} + \frac{\ddot{H}}{H^3} \equiv 1 + 3\Upsilon(z) + \Theta(z), \tag{27}$$

$$s = -\frac{6\dot{H}/H^2 + 2\ddot{H}/H^3}{9 + 6\dot{H}/H^2} \equiv -\frac{6\Upsilon(z) + 2\Theta(z)}{9 + 6\Upsilon(z)}, \tag{28}$$

where

$$\begin{aligned}\Upsilon(z) &= \frac{\dot{H}}{H^2} \\ &= -\frac{3}{2} - \frac{3}{2}\omega_{\mathrm{DE}}\Omega_{0\mathrm{DE}}(1+z)^{3\omega_{\mathrm{DE}}(1+\alpha)}\,(1-\Omega_{0B})^{\alpha/(1+\alpha)} \\ &\quad\times\left\{(1-\Omega_{0\mathrm{B}})^{\alpha/(1+\alpha)}\left[\Omega_{0\mathrm{DM}}+\Omega_{0\mathrm{DE}}(1+z)^{3\omega_{\mathrm{DE}}(1+\alpha)}\right]\right. \\ &\quad\left.+\Omega_{0\mathrm{B}}\left[\Omega_{0\mathrm{DM}}+\Omega_{0\mathrm{DE}}(1+z)^{3\omega_{\mathrm{DE}}(1+\alpha)}\right]^{\alpha/(1+\alpha)}\right\}^{-1},\end{aligned} \tag{29}$$

and

$$\begin{aligned}\Theta(z) &= \frac{\ddot{H}}{H^3} \\ &= \frac{9}{2} + \frac{9}{2}(1-\Omega_{0\mathrm{B}})^{\alpha/(1+\alpha)} \\ &\quad\times\left\{2\omega_{\mathrm{DE}}\Omega_{0\mathrm{DE}}(1+z)^{3\omega_{\mathrm{DE}}(1+\alpha)}\right. \\ &\quad+(1+\alpha)\,\omega_{\mathrm{DE}}^2\Omega_{0\mathrm{DE}}(1+z)^{3\omega_{\mathrm{DE}}(1+\alpha)} \\ &\quad-\alpha\omega_{\mathrm{DE}}^2\Omega_{0\mathrm{DE}}^2(1+z)^{6\omega_{\mathrm{DE}}(1+\alpha)} \\ &\quad\left.\times\left[\Omega_{0\mathrm{DM}}+\Omega_{0\mathrm{DE}}(1+z)^{3\omega_{\mathrm{DE}}(1+\alpha)}\right]^{-1}\right\} \\ &\quad\times\left\{(1-\Omega_{0\mathrm{B}})^{\alpha/(1+\alpha)}\left[\Omega_{0\mathrm{DM}}+\Omega_{0\mathrm{DE}}(1+z)^{3\omega_{\mathrm{DE}}(1+\alpha)}\right]\right. \\ &\quad\left.+\Omega_{0\mathrm{B}}\left[\Omega_{0\mathrm{DM}}+\Omega_{0\mathrm{DE}}(1+z)^{3\omega_{\mathrm{DE}}(1+\alpha)}\right]^{\alpha/(1+\alpha)}\right\}^{-1}.\end{aligned} \tag{30}$$

Then, the evolution trajectories of our model in the plane of the Statefinder parameters can also be plotted (see Figs. 5 and 6).

Since different dark energy models have distinct evolution trajectories in the plane of the Statefinder parameters, we can distinguish between various dark energy models and the MGCG. Just as the literatures [56, 58] show: The ΛCDM scenario corresponds to the fixed point $\{r = 1, s = 0\}$; the standard cold dark matter scenario corresponds to the point $\{r = 1, s = 1\}$; the Statefinder parameters plane of quiessence are some vertical segments where r decreases monotonically from 1 to $1 + \frac{9}{2}\omega_{\mathrm{DE}}(1 + \omega_{\mathrm{DE}})$ and s remains constant at $1 + \omega_{\mathrm{DE}}$; the quintessence tracker models have typical trajectories similar to arcs of an upward parabola lying in the regions $\{r < 1, s > 0\}$.

Now, we can see the Statefinder parameters plane of the MGCG from Figs. 5 and 6. In Fig. 5, we fix $\alpha = 0.5$ and vary ω_{DE} as -1.05, -1.00, -0.95, and -0.90, respectively. Where $\omega_{\mathrm{DE}} = -1.00$ exhibits a complete downward parabola, while the others correspond to some broken parabolas. And from this diagram, we can see the Statefinder trajectory begins with $r = 1$. Besides, the cases of $\omega_{\mathrm{DE}} < -1$ never arrive at the fixed point $\{1, 0\}$, and when $\omega_{\mathrm{DE}} > -1$, the trajectories must pass through this point. Finally, we can see that the less ω_{DE}, the smaller today's value s_0 and the larger today's

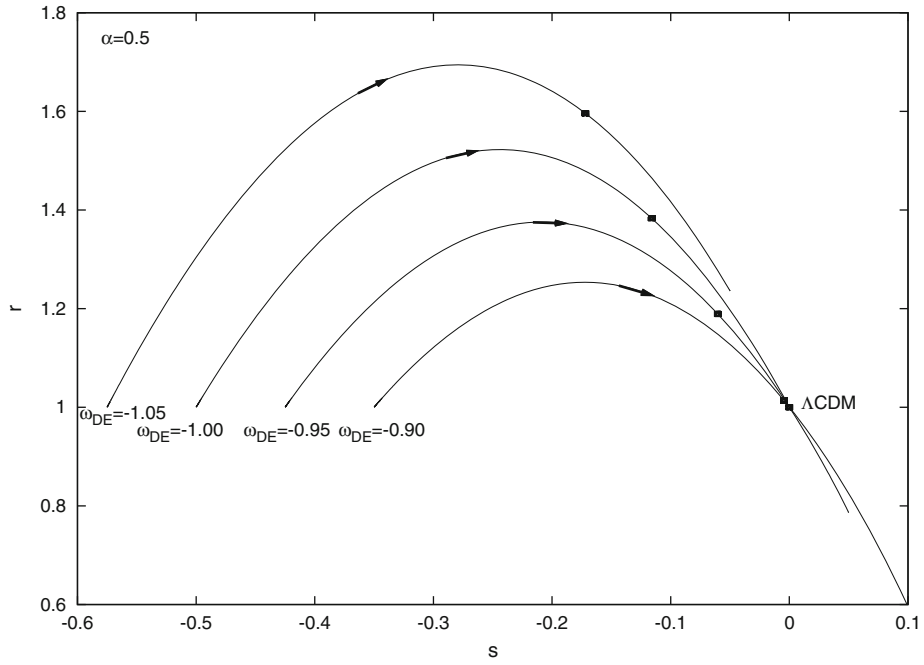

Fig. 5 The Statefinder $r(s)$ evolution diagram when we fix α and vary $\omega_{\rm DE}$. *Dots* locate today's values and *arrows* denote the direction of evolution for the MGCG

value r_0. However, in Fig. 6, we fix $\omega_{\rm DE} = -0.85$ and vary α as 3.1, 2.7, 2.3, 1.9, 1.51, 1.1, and 0.7, respectively. It is interesting to see that the trajectories can pass through the fixed point $\{1, 0\}$. And when fixed $\omega_{\rm DE}$, the less α, the smaller today's value s_0 and the larger today's value r_0. We notice the present Statefinder points as well as the fixed point $\{1, 0\}$ locate on a straight line which means the relationship between r_0 and s_0 is linear

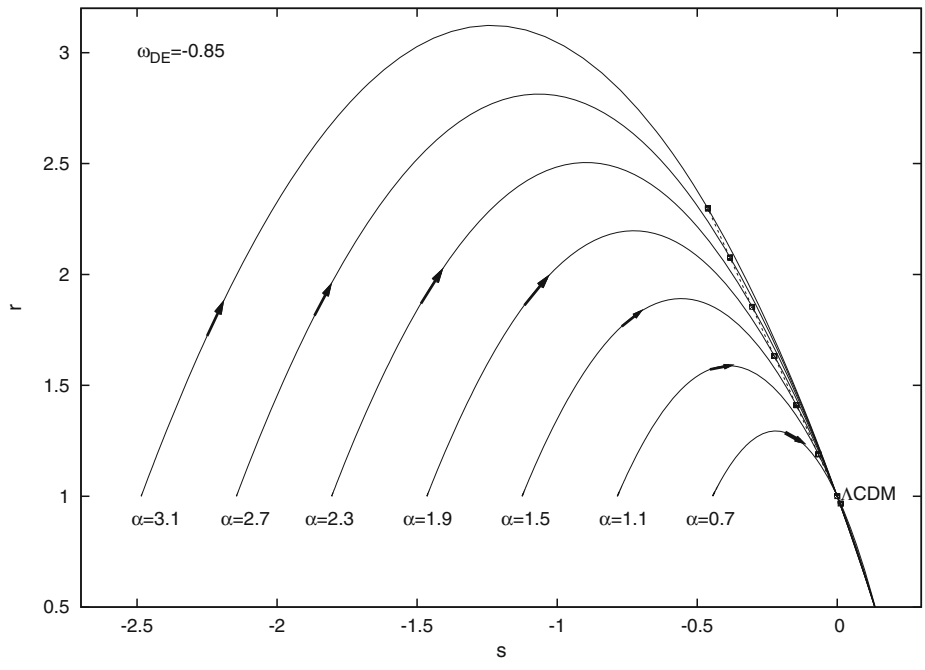

Fig. 6 The Statefinder $r(s)$ evolution diagram when we fix $\omega_{\rm DE}$ and vary α. *Dots* locate today's values and *arrows* denote the direction of evolution for the MGCG

when we fix $\omega_{\rm DE}$. That is because of the following relationships:

$$r_0 = 1 + \frac{9}{2}\omega_{\rm DE}\Omega_{0\rm DE}\left[1 + (1+\alpha)\,\omega_{\rm DE} - \frac{\alpha\omega_{\rm DE}\Omega_{0\rm DE}}{1-\Omega_{0\rm B}}\right],$$

$$s_0 = 1 + (1+\alpha)\,\omega_{\rm DE} - \frac{\alpha\omega_{\rm DE}\Omega_{0\rm DE}}{1-\Omega_{0\rm B}}, \tag{31}$$

so that

$$r_0 = 1 + \frac{9}{2}\omega_{\rm DE}\Omega_{0\rm DE}s_0. \tag{32}$$

The above separation between distinct families of dark energy models is very remarkable when we analyze evolutionary trajectories using the Statefinder pair $\{r, s\}$. Forthcoming space-based missions such as SNAP are expected to greatly increase and improve the current type Ia supernovae inventory and maybe can identify which kind of dark energy model.

4 Constraints on MGCG

4.1 The Sound Speed

Since our model can be considered as a new scenario for unified dark matter and dark energy, we have to study its density perturbations and the structure formation, and we also have to investigate its adiabatic sound speed. So, in this section, we consider some effective parameters for the MGCG such as α and $\omega_{\rm DE}$ by the maximum likelihood estimation. If the MGCG is considered as a perfect fluid satisfying (2), then the MGCG component will cluster gravitationally with the adiabatic sound speed given by

$$\begin{aligned} c_{\rm s}^2 &\equiv \frac{\partial p}{\partial \rho} \\ &= -\frac{\alpha}{1+\alpha} - \frac{\alpha}{1+\alpha}\frac{\Omega_{0\rm DE}\left[\omega_{\rm DE} + \alpha\left(1+\omega_{\rm DE}\right)\right](1+z)^{3\omega_{\rm DE}(1+\alpha)} + \alpha\Omega_{0\rm DM}}{\Omega_{0\rm DE}(1+z)^{3\omega_{\rm DE}(1+\alpha)} + \Omega_{0\rm DM}} \\ &\quad + \frac{\left(1+\omega_{\rm DE}\right)\Omega_{0\rm DE}\left[\omega_{\rm DE} + \alpha\left(1+\omega_{\rm DE}\right)\right](1+z)^{3\omega_{\rm DE}(1+\alpha)} + \alpha\Omega_{0\rm DM}}{\left(1+\omega_{\rm DE}\right)\Omega_{0\rm DE}(1+z)^{3\omega_{\rm DE}(1+\alpha)} + \Omega_{0\rm DM}}. \end{aligned} \tag{33}$$

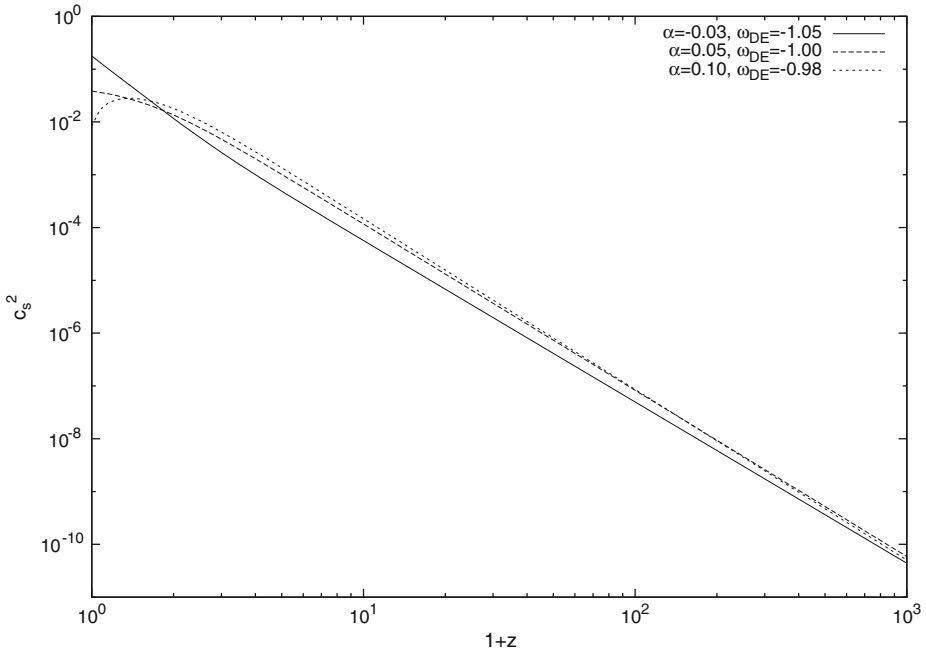

Fig. 7 The evolution of the sound speed squared of the MGCG as a function of redshift for $\alpha = -0.03$, 0.05, and 0.10

From the above equation, we obtain $\alpha \neq -1$. However, when $\alpha < -1$, we can derive $c_s^2|_{z\to\infty} \simeq \omega_{DE} < 0$, and when c_s^2 is negative, the MGCG fluid is unstable. When $\alpha > -1$, we have $c_s^2|_{z\to\infty} \simeq 0$. Thus, the parameter α must be greater than -1 because the limit of the sound speed was very small at early time and cannot be larger than 1 even though in the future if our model can be as the unified dark matter–dark energy. From Fig. 7, we can see that the slope of the curves for c_s^2 depends on α and ω_{DE}. Besides, we clearly see that deep in the matter era, the behavior of the MGCG closely resembles that of CDM.

To constrain α and ω_{DE} further, combined with the data of SNe Ia, CMB, and 2dFGRS, it imposes a range on ω_{DE}: $-1.46 < \omega_{DE} < -0.78$ [48, 49]. Through the limit of the sound speed $0 < c_s^2 < 1$, when we use Eq. (33), we can find the domain of $\alpha - \omega_{DE}$ plane (see Fig. 8). Then, we derive $-0.3 < \alpha < 4.7$ and $-1.19 < \omega_{DE} < -0.78$. From Fig. 8, we can see that the boundary of domain is constrained by the sound speed.

4.2 The Age of the Universe

By using a distance-independent method, Jimenez et al. [60] determined the age of globular clusters in the Milky Way as $t_0 = 13.5 \pm 2$ Gyr. By using the white dwarfs cooling sequence method, Richer et al. [61] and Hansen et al. [62] constrained the age of the globular cluster M4 to be $t_0 = 12.7 \pm 0.7$ Gyr. Then, the age of the universe needs to satisfy the lower bound: $t_0 > 11$–12 Gyr. Assuming ΛCDM, WMAP7 data give the age of the universe $t_0 = 13.73 \pm 0.13$ Gyr [50]. Here we adopt model-independent astronomical observations of globular clusters as a criterion. Making use of the definition for the Hubble parameter $H = \dot{a}/a$ and the relationship between the scale factor and the redshift $1 + z = 1/a$, then we have

$$\mathrm{d}t = \frac{\mathrm{d}a}{aH} = -\frac{1}{(1+z)H}\mathrm{d}z. \tag{34}$$

Integrating the above equation, we obtain

$$\begin{aligned} t_0 &= \int_0^{t_0} \mathrm{d}t = \int_0^{\infty} \frac{\mathrm{d}z}{H(1+z)} \\ &= \frac{1}{H_0}\int_0^{\infty} \frac{\mathrm{d}z}{(1+z)^{5/2}\sqrt{(1-\Omega_{0B})^{\frac{\alpha}{1+\alpha}}\left[\Omega_{0DM} + \Omega_{0DE}(1+z)^{3\omega_{DE}(1+\alpha)}\right]^{\frac{1}{1+\alpha}} + \Omega_{0B}}}. \end{aligned} \tag{35}$$

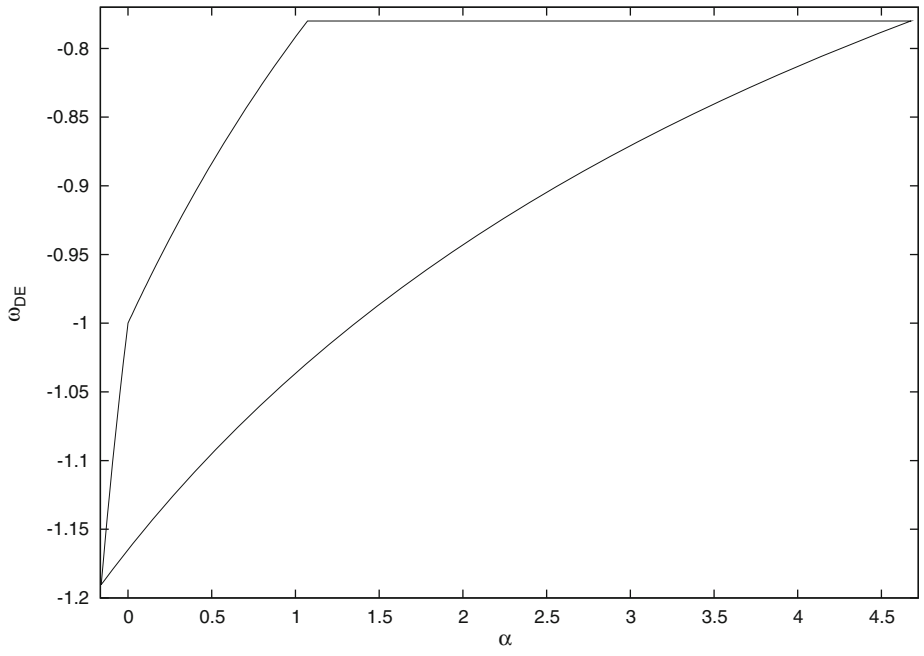

Fig. 8 The region inside the curve is the domain of parameters α and ω_{DE} which is constrained by the sound speed

In Fig. 9, with using the age data of the universe, we plot the isochrones in α - $\omega_{\rm DE}$ plane under the boundary of domain constrained by $c_{\rm s}^2$. Then, we can see that the parameters α and $\omega_{\rm DE}$ are constrained by the age of the universe further. Since the luminosity distance for all models is given by the simple expression for a spatially flat universe

$$H(z) = \left[\frac{d}{{\rm d}z}\left(\frac{D_{\rm L}(z)}{1+z}\right)\right]^{-1}, \tag{36}$$

using the (35) and (36), we have

$$t_0 = \frac{D_{\rm L}}{(1+z)^2}\bigg|_0^\infty + \int_0^\infty \frac{D_{\rm L}}{(1+z)^3}{\rm d}z. \tag{37}$$

From above equation, we can see that the luminosity distance is directly related to the age of the universe.

4.3 The Linear Density Perturbations

In this subsection, we will study the growth of density perturbations for the MGCG fluid in the linear regime on subhorizon scales. We will follow the analysis method in [28–33]. Firstly, we will introduce some quantities used in this part. The relationship between the comoving coordinate $(\vec{x}, t)$ and the physical coordinate $(\vec{r}, t)$ is $\vec{x} = \vec{r}/a$. The velocity in physical coordinate is $\vec{u} = \dot{\vec{r}}$. Furthermore, we can expand $\vec{u} = \dot{a}\vec{x} + \vec{v}$ where $\vec{v}$ is the first-order perturbation to the Hubble flow $\dot{a}\vec{x}$. $\rho_{\rm DM}(\vec{x}, t) = \rho_{0\rm DM}(t)(1 + \delta_{\rm DM}(\vec{x}, t))$ where $\rho_{0\rm DM}(t)$ is the background density and $\delta_{\rm DM}(\vec{x}, t)$ is the first-order perturbation of $\rho_{0\rm DM}$. $\phi(\vec{x}, t)$ is the first-order perturbation of Newtonian potential Φ, which satisfies Poisson's equation $\nabla^2\Phi = 4\pi G a^2 \rho_{\rm DM}$ in the comoving coordinate.

Before discussing the linear density perturbations, we will research an explicit interaction between dark matter and dark energy in our model and depict this interaction through an energy exchange term Γ which will be used in the linear density perturbed equations. From (10) and (11), we can obtain the scaling behavior of the energy densities as follows:

$$\frac{\rho_{\rm DM}}{\rho_{\rm DE}} = \frac{\kappa}{\lambda}(1+z)^{-3\omega_{\rm DE}(1+\alpha)} = \frac{\Omega_{0\rm DM}}{\Omega_{0\rm DE}}(1+z)^{-3\omega_{\rm DE}(1+\alpha)}, \tag{38}$$

where there is an explicit interaction between dark matter and dark energy. This can be seen from the energy conservation equation more clearly, which can be written as

$$\dot{\rho}_{\rm DM} + 3H\rho_{\rm DM} = -\left[\dot{\rho}_{\rm DE} + 3H\left(\rho_{\rm DE} + p_{\rm DE}\right)\right]. \tag{39}$$

Furthermore,

$$\dot{\rho}_{\rm DM} + 3H\rho_{\rm DM} = \Gamma, \tag{40}$$

$$\dot{\rho}_{\rm DE} + 3H\left(\rho_{\rm DE} + p_{\rm DE}\right) = -\Gamma, \tag{41}$$

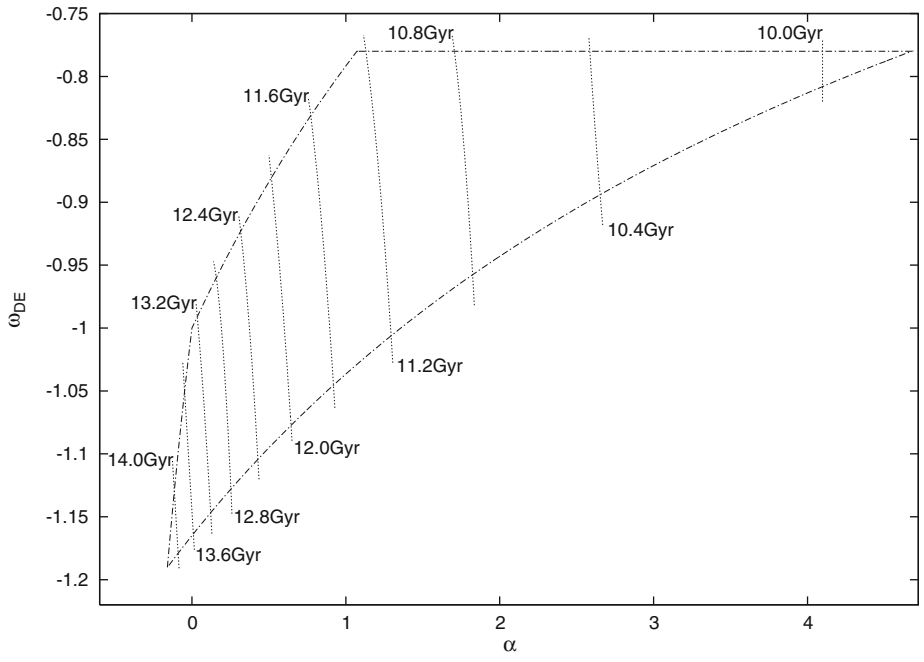

Fig. 9 The *dashed-dot curve* is the domain of parameters α and $\omega_{\rm DE}$ which is constraints from the sound speed. The *dot line* is the isochrones for parameter t_0 in the α-$\omega_{\rm DE}$ plane

where Γ is the source term in the continuity equation due to the energy transferring between dark matter and quiessence dark energy in our model. From the above equations, we can, respectively, derive the effective equations of state for dark matter $\omega_{\rm DM}^{\rm eff}$ and dark energy $\omega_{\rm DE}^{\rm eff}$ in the MGCG scenario

$$\omega_{\rm DM}^{\rm eff} = -\frac{\Gamma}{3H\rho_{\rm DM}} = -\frac{\alpha\omega_{\rm DE}\Omega_{0\rm DE}(1+z)^{3\omega_{\rm DE}(1+\alpha)}}{\Omega_{0\rm DM}+\Omega_{0\rm DE}(1+z)^{3\omega_{\rm DE}(1+\alpha)}}, \tag{42}$$

$$\omega_{\rm DE}^{\rm eff} = \omega_{\rm DE} + \frac{\Gamma}{3H\rho_{\rm DE}} = \omega_{\rm DE}(1+\alpha) - \frac{\alpha\omega_{\rm DE}\Omega_{0\rm DE}(1+z)^{3\omega_{\rm DE}(1+\alpha)}}{\Omega_{0\rm DM}+\Omega_{0\rm DE}(1+z)^{3\omega_{\rm DE}(1+\alpha)}}. \tag{43}$$

Now, we focus on the mass density perturbations in the linear approximation. In this paper, we apply the comoving coordinate $(\vec{x}, t)$ for a pressureless fluid with background density $\rho_{0\rm DM}$ and density contrast $\delta_{\rm DM}$, with a source term Γ due to the energy transfer from dark matter to quiessence dark energy. Based on [63], in the first-order approximation, the perturbed equations are written in the comoving coordinate as follows:

$$\frac{\partial\vec{v}}{\partial t} + \frac{\dot{a}}{a}\vec{v} = -\frac{\nabla\phi}{a}, \tag{44}$$

$$\nabla\cdot\vec{v} = -a\frac{\partial\delta_{\rm DM}}{\partial t} - a\Gamma\frac{\delta_{\rm DM}}{\rho_{0\rm DM}}, \tag{45}$$

$$\frac{1}{a^2}\nabla^2\phi = 4\pi G\rho_{0\rm DM}\delta_{\rm DM}, \tag{46}$$

where $\delta_{\rm DM}$, $\vec{v}$, and ϕ are, respectively, the first-order perturbations of $\rho_{0\rm DM}$, $\dot{a}\vec{x}$, and the Newtonian potential Φ. Since the matter is so cold, the term proportional to the speed of sound $c_{\rm s}^2$ in (44) can be omitted. It leads to disappearance of the term $\frac{c_{\rm s}^2}{a}\nabla\delta_{\rm DM}$ in (44) [64]. Assume that both the density contrast $\delta_{\rm DM}$ and peculiar velocity $\vec{v}$ are small, i.e., $\delta_{\rm DM}\ll 1$ and $\vec{v}\ll\vec{u}$, where $\vec{u}$ is the velocity in physical coordinate. Taking the divergence of (44) and substituting (45) and (46), we finally obtain

$$H^2\delta_{\rm DM}'' + \left(\dot{H}+2H^2+H\frac{\Gamma}{\rho_{\rm DM}}\right)\delta_{\rm DM}' - \left[4\pi G\rho_{\rm DM} - 2H\frac{\Gamma}{\rho_{\rm DM}} - H\left(\frac{\Gamma}{\rho_{\rm DM}}\right)'\right]\delta_{\rm DM} = 0, \tag{47}$$

where $' \equiv d/d\ln a$. Since the term $\frac{c_{\rm s}^2}{a}\nabla\delta_{\rm DM}$ is not included in the Euler equation, it leads to disappearance of the term $\nabla^2\delta_{\rm DM}$ in (47). And we can easily see that there is no scale-dependent term to drive oscillations or blowup in the power spectrum. We can solve (47) numerically; when the initial conditions are chosen as $a = 10^{-3}$ and $\delta_{\rm DM}\simeq 10^{-3}$, we plot the linear density perturbation for dark matter $\delta_{\rm DM}$ as a function of a

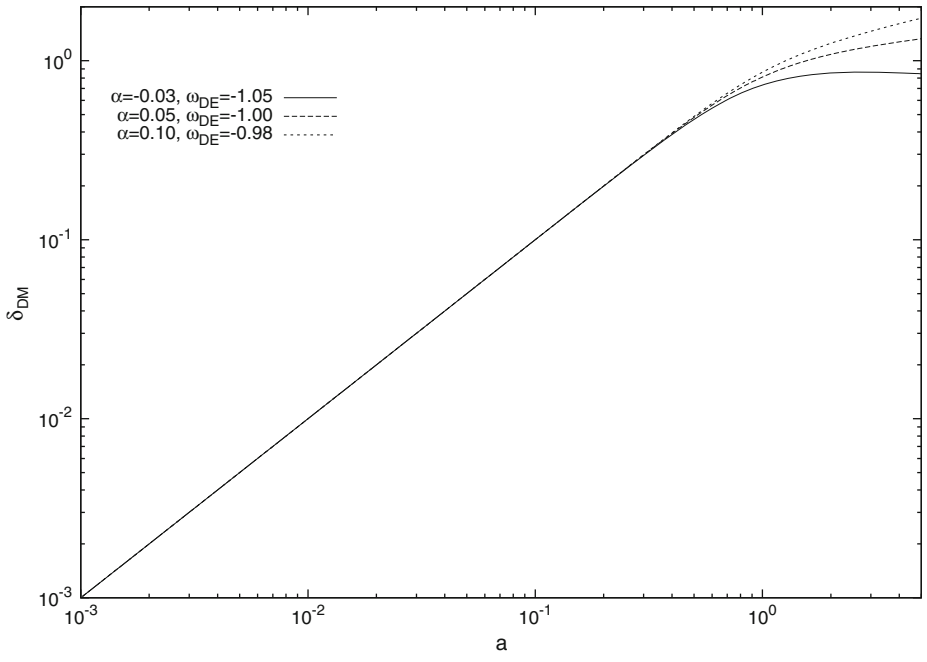

Fig. 10 $\delta_{\rm DM}$ as the function of scale factor a

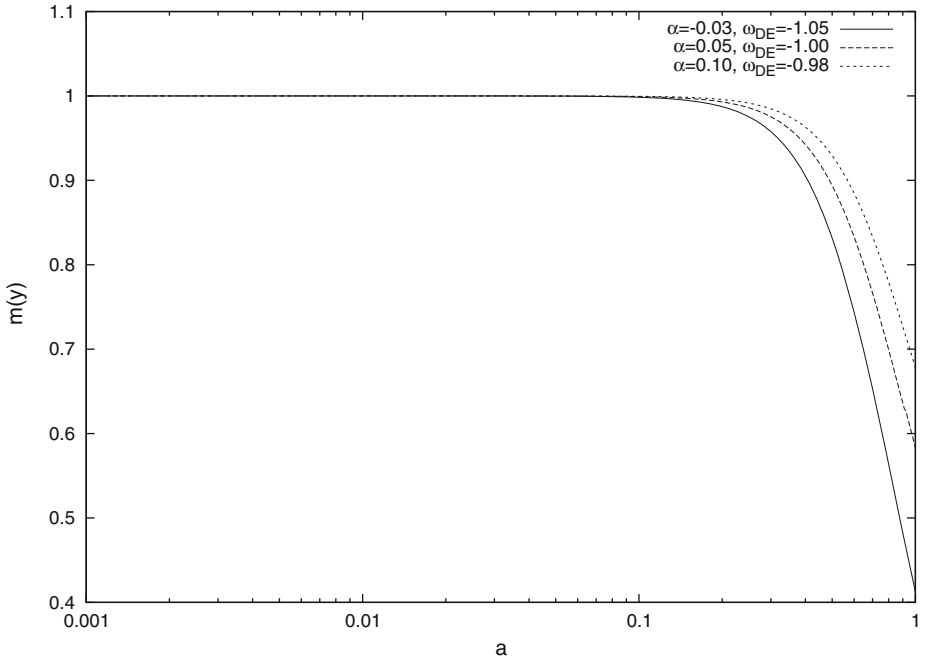

Fig. 11 The growth factor $m(y)$ as a function of scale factor a

(see Fig. 10). In Fig. 10, we can see the perturbation starts departing from the linear behavior around $a \simeq 0.80$, i.e., $z \simeq 0.25$ which is similar to the epoch when $z < z_{\rm eq}$. Through the energy transferring from dark matter to dark energy, we can see that the dominance of dark energy is related to the time when the density fluctuations start deviating from the linear behavior.

When we consider the period after decoupling, the baryons are no longer coupled to photons so that the baryons are also a pressureless fluid like the dark

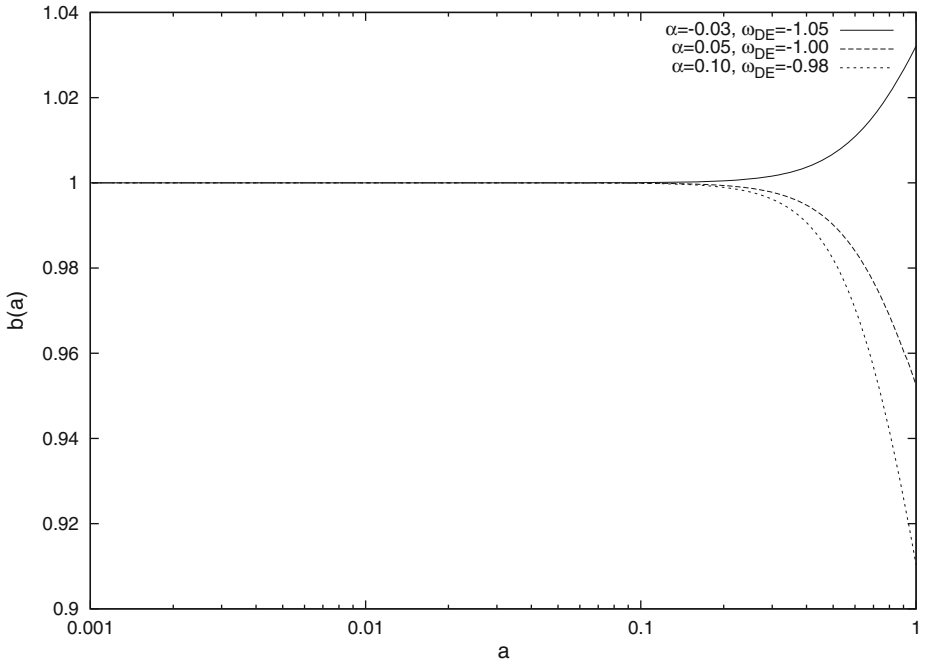

Fig. 12 The bias $b\,(a)$ as a function of scale factor a

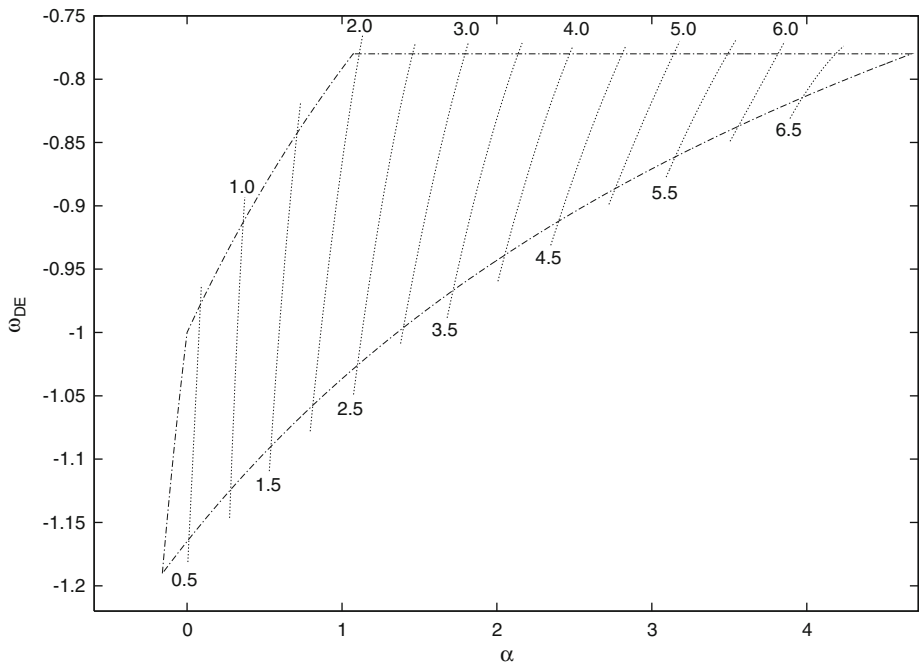

Fig. 13 The contours for growth factor m in the $\alpha - \omega_{\rm DE}$ plane

matter. Then, we derive the baryon perturbation as follows:

$$H^2\delta_{\rm B}'' + (\dot{H} + 2H^2)\delta_{\rm B}' - 4\pi G\rho_{\rm DM}\delta_{\rm DM} = 0. \quad (48)$$

Then we investigate the growth factor $m(y)$ and the bias $b(a)$ where $m(y) = D'(y)/D(y)$, $D(y)$ is the linear growth function, $y = \ln(a)$ and $b = \delta_{\rm B}/\delta_{\rm DM}$. One can see from Figs. 11 and 12 that between the present and $z \simeq 5$, the growth factor $m(y)$ and the bias $b(a)$

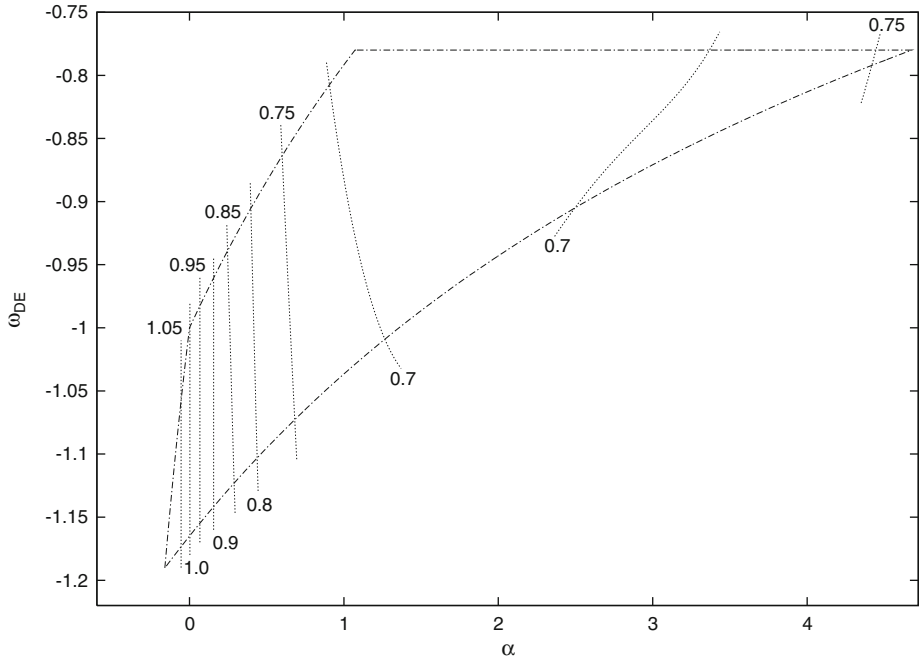

Fig. 14 The contours for bias b in the $\omega_{\rm DE} - \alpha$ plane

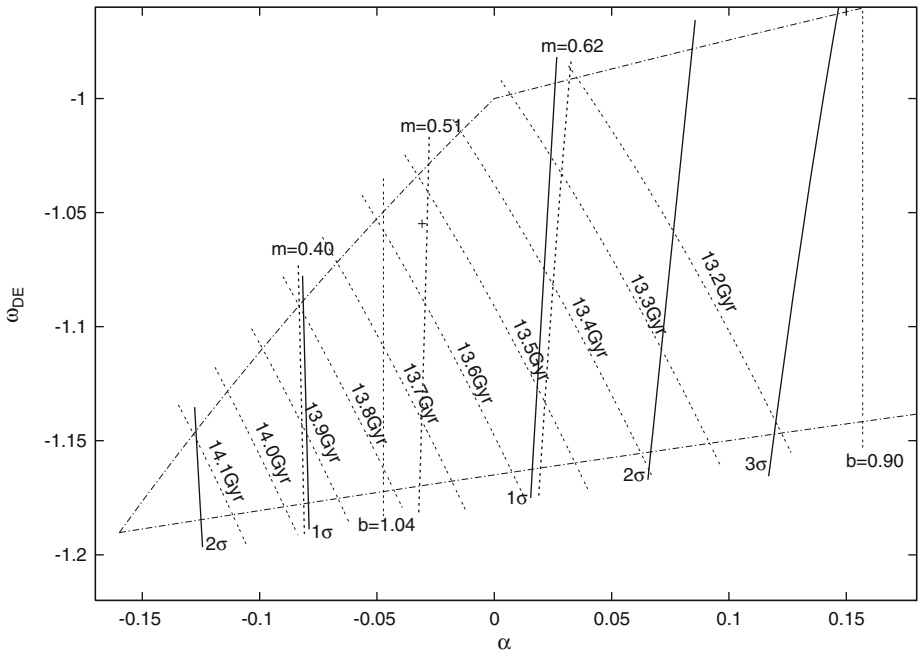

Fig. 15 The contours in *solid lines* come from four limits of c_s^2, t_0, m, and b in the $\omega_{DE} - \alpha$ plane. The confidence levels show the contours of 68.3%, 95.4%, and 99.73%. The 1σ fit values for our model parameters are $\alpha = -3.07^{+5.66}_{-4.98} \times 10^{-2}$ and $\omega_{DE} = -1.05^{+0.06}_{-0.11}$. And the *plus sign* in this figure denotes the best fits

are quite sensitive to the values of α and ω_{DE}. Subsequently, we consider the constraints from $m(y)$ and $b\,(a)$ on the $\alpha - \omega_{DE}$ plane. In Figs. 13 and 14, we have shown the contours for the growth factor $m(y)$ and the bias $b\,(a)$ in the $\alpha - \omega_{DE}$ plane under the boundary of domain constrained by c_s^2. On the other hand, the growth factor and the bias parameter at $z \simeq 0.15$ have been determined using the 2dFGRS. The redshift space distortion parameter $\beta = 0.49 \pm 0.09$ and the bias $b = 1.04 \pm 0.11$ [65–67]. For $\beta = m/b$, we can subsequently determine the constraint on the growth factor m as $m = 0.51 \pm 0.11$. Note that the fitted values of b and β are sensitive to the underlying model and the observational constraints on them are obtained under ΛCDM when converting redshift to distances for the power spectra. The right way is to conduct data processing for b and β by using 2dFGRS data under our model. Then we can constrain α and ω_{DE} by using the fitted values. In this paper, we use the above fitted data temporarily, and our future work will focus on this difficult task.

In Fig. 15, we consider four restrictions together to give the best estimation of α and ω_{DE}. Firstly, we plot contours constraint imposed by t_0 (Fig. 9), m (Fig. 13), and b (Fig. 14) under the boundary of domain constrained by the sound speed. Each set leads to a reduced χ^2: $\chi^2(\alpha, \omega_{DE})$ = (theory values − observation values)^2/(observational error)^2. To combine the constraints on α and ω_{DE} coming from the age of the universe t_0, growth factor m, and the bias b within the domain given by the limits of the sound speed c_s^2, we have added their individual χ^2 as if they were part of a total experiment with uncorrelated Gaussian errors: $\chi^2_{total}(\alpha, \omega_{DE}) = \chi^2_{t_0}(\alpha, \omega_{DE}) + \chi^2_m(\alpha, \omega_{DE}) + \chi^2_b(\alpha, \omega_{DE})$. Therefore, we plot the contour level $\Delta\chi^2_{total}(\alpha, \omega_{DE}) = 2.3$, $\Delta\chi^2_{total}(\alpha, \omega_{DE}) = 6.17$, and $\Delta\chi^2_{total}(\alpha, \omega_{DE}) = 11.8$, where $\Delta\chi^2_{total}(\alpha, \omega_{DE}) = \chi^2(\alpha, \omega_{DE}) - (\chi^2(\alpha, \omega_{DE}))_{min}$ defines, respectively, for 2 degrees of freedom the 68.3%, 95.4%, and 99.73% confidence levels represented in Fig. 15. The 1σ fit values are $\alpha = -3.07^{+5.66}_{-4.98} \times 10^{-2}$ and $\omega_{DE} = -1.05^{+0.06}_{-0.11}$. Note that the presence of the cutoff contours' curves in Fig. 15 is due to the restricted area boundary which comes from the limits of c_s^2.

5 Conclusion

A new model named as the MGCG, which is a further generalization of the generalized Chaplygin gas, has been proposed in the present paper. As a version of the unified dark matter and dark energy, this MGCG fluid is consisted of dark matter and quiessence dark energy with constant ω_{DE}. Firstly, fundamental cosmology equations for the MGCG have been described. For tests with future deep observations, we then consider the Statefinder diagnostic since it can probe the expansion dynamics of the universe through higher derivatives of the scale factor. Furthermore, we investigate

the evolution of density perturbations and the structure formation in our model. Then, when we apply the age of the universe data t_0, growth factor m, and the bias b within the domain given by the limits of c_s^2, the parameters α and ω_{DE} are constrained: $\alpha = -3.07^{+5.66}_{-4.98} \times 10^{-2}$ and $\omega_{DE} = -1.05^{+0.06}_{-0.11}$. It has been shown that there are few differences between our model and the others. To determine whether our model could be a candidate model of dark energy, the analysis and discussion of the matter power spectrum for MGCG must be done. This is a subject of our future research.

Acknowledgements X.-M. Deng thanks the suggestions and comments from a referee, which plays an important role for the improvement of this article. X.-M. Deng appreciates the support from the group of Almanac and Astronomical Reference Systems in the Purple Mountain Observatory of China.

References

1. A. G. Riess et al., Astron. J. **116**, 1009 (1998)
2. S. Perlmutter et al., Astrophys. J. **517**, 565 (2003)
3. J. L. Tonry et al., Astrophys. J. **594**, 1 (2003)
4. D. N. Spergel et al., Astrophys. J. Suppl. **148**, 175 (2003)
5. C. L. Bennett et al., Astrophys. J. Suppl. **148**, 1 (2003)
6. M. Tegmark et al., Astrophys. J. **606**, 702 (2004)
7. S. Weinberg, Rev. Mod. Phys. **61**, 1 (1989)
8. P. J. E. Peebles, B. Ratra, Rev. Mod. Phys. **75**, 559 (2003)
9. B. Ratra, P. J. E. Peebles, Phys. Rev. D **37**, 3406 (1998)
10. R. R. Caldwell, R. Dave, P. J. Steinhardt, Phys. Rev. Lett. **80**, 1582 (1998)
11. M. Sami, T. Padmanabhan, Phys. Rev. D **67**, 083509 (2003)
12. C. Armendariz-Picon, V. Mukhanov, P. J. Steinhardt, Phys. Rev. D **63**, 103510 (2001)
13. T. Chiba, Phys. Rev. D **66**, 063514 (2002)
14. R. J. Scherrer, Phys. Rev. Lett. **93**, 011301 (2004)
15. A. Sen, J. High Energy Phys. **04**, 048 (2002)
16. A. Sen, J. High Energy Phys. **07**, 065 (2002)
17. G. W. Gibbons, Phys. Lett. B **537**, 1 (2002)
18. R. R. Caldwell, Phys. Lett. B **545**, 23 (2002)
19. E. Elizalde, S. Nojiri, S. D. Odintsov, Phys. Rev. D **70**, 043539 (2004)
20. J. M. Cline, S. Jeon, G. D. Moore, Phys. Rev. D **70**, 043543 (2004)
21. B. Feng, M. Li, Y. Piao, X. Zhang, Phys. Lett. B **634**, 101 (2006)
22. Z. Guo, Y. Piao, X. Zhang, Y. Zhang, Phys. Rev. D **74**, 127304 (2006)
23. S. Kachru, M. Schulz, E. Silverstein, Phys. Rev. D **62**, 045021 (2000)
24. S. M. Carroll, L. Mersini, Phys. Rev. D **64**, 124008 (2001)
25. S. Kachru, R. Kallosh, A. Linde, S. P. Trivedi, Phys. Rev. D **68**, 046005 (2003)
26. S. Carroll et al., Phys. Rev. D **70**, 043528 (2004)
27. C. Deffayet, G. Dvali, G. Gabadadze, Phys. Rev. D **65**, 044023 (2002)
28. M. C. Bento, O. Bertolami, A. A. Sen, Phys. Rev. D **66**, 043507 (2002)
29. M. C. Bento, O. Bertolami, A. A. Sen, Phys. Rev. D **67**, 063003 (2003)
30. M. C. Bento, O. Bertolami, A. A. Sen, Phys. Rev. D **70**, 083519 (2004)
31. M. C. Bento, O. Bertolami, N. M. C. Santos, A. A. Sen, Phys. Rev. D **71**, 063501 (2005)
32. A. A. Sen, R. J. Scherrer, Phys. Rev. D **72**, 063511 (2005)
33. R. Banerjee, S. Ghosh, S. Kulkarni, Phys. Rev. D **75**, 025008 (2007)
34. M. Bouhmadi-López, P. V. Moniz, Phys. Rev. D **71**, 063521 (2005)
35. T. Giannantonio, A. Melchiorri, Class. Quantum Gravity **23**, 4125 (2006)
36. G. A. Monerat et al., Phys. Rev. D **76**, 024017 (2007)
37. M. Heydari-Fard, H. R. Sepangi, Phys. Rev. D **76**, 104009 (2007)
38. P. T. Silva, O. Bertolami, Astrophys. J. **599**, 829 (2003)
39. O. Bertolami, A. A. Sen, S. Sen, P. T. Silva, Mon. Not. R. Astron. Soc. **353**, 329 (2004)
40. E. J. Copeland, M. Sami, S. Tsujikawa, Int. J. Mod. Phys. D **15**, 1753 (2006)
41. L. P. Chimento, Phys. Rev. D **69**, 123517 (2004)
42. X. Zhang, F. Q. Wu, J. J. Zhang, Cosmol. Astropart. Phys. **01** 003 (2006)
43. G. Aldering et al., SPIE **4835**, 146A (2002)
44. A. Kamenshchik, U. Moschella, V. Pasquier, Phys. Lett. B **511**, 265 (2001)
45. H. Sandvik, M. Tegmark, M. Zaldarriaga, I. Waga, Phys. Rev. D **69**, 123524 (2004)
46. V. Sahni, Lect. Notes Phys. **653**, 141 (2004)
47. L. P. Chimento, R. Lazkoz, Class. Quant. Grav. **23**, 3195 (2006)
48. R. A. Knop et al., Astrophys. J. **598**, 102 (2003)
49. A. G. Riess et al., Astrophys. J. **607**, 665 (2004)
50. N. Jarosik et al., Astrophys. J. Suppl. **192**, 14 (2011)
51. M. Colless et al., Mon. Not. R. Astron. Soc. **328**, 1039 (2001)
52. J. D. Barrow, R. Bean, J. Magneijo, Mon. Not. R. Astron. Soc. **316**, 41 (2000)
53. M. Tegmark et al., Phys. Rev. D **69**, 103501 (2004)
54. S. Podariu, R. A. Daly, M. P. Mory, B. Ratra, Astrophys. J. **584**, 577 (2003)
55. V. Gorini, A. Y. Kamenshchik, U. Moschella, O. F. Pisttella, A. A. Starobinsky, J. Cosmol. Astropart. Phys. **02**, 016 (2008)
56. V. Sahni, T. D. Saini, A. A. Starobinsky, U. Alam, JETP Lett. **77**, 201 (2003)
57. U. Alam, V. Sahni, T. D. Saini, A. A. Starobinsky, Mon. Not. R. Astron. Soc. **344**, 1057 (2003)
58. V. Gorini, A. Kamenshchik, U. Moschella, Phys. Rev. D **67**, 063509 (2003)
59. W. Zimdahl, D. Pavon, Gen. Relativ. Gravit. **36**, 1483 (2004)
60. R. Jimenez, P. Thejll, U. Jorgensen, J. MacDonald, B. Pagel, Mon. Not. R. Astron. Soc. **282**, 926 (1996)
61. H. Richer et al., Astrophys. J. **574**, L151 (2002)
62. B. Hansen et al., Astrophys. J. **574**, L155 (2002)
63. R. C. Arcuri, I. Waga, Phys. Rev. D **50**, 2928 (1994)
64. V. Mukhanov, *Physical Foundations of Cosmology* (Cambridge University Press, Cambridge, 2005)
65. L. Verde et al., Mon. Not. R. Astron. Soc. **335**, 432 (2002)
66. E. Hawkins et al., Mon. Not. R. Astron. Soc. **346**, 78 (2003)
67. E. V. Linder, Astropart. Phys. **29**, 336 (2008)